Low-frequency magnetic sensing by magnetoelectric metglas/bidomain LiNbO₃ long bars

Andrei V. Turutin[1,2], João V. Vidal[3], Ilya V. Kubasov[1], Alexander M. Kislyuk[1], Mikhail D. Malinkovich[1], Yurii N. Parkhomenko[1], Svetlana P. Kobeleva[1], Andrei L. Kholkin[3,4], and Nikolai A. Sobolev[1,2]

[1] - National University of Science and Technology MISiS, Moscow, 119049, Leninsky av. 4, Russia
[2] - Department of Physics and I3N, University of Aveiro, 3810-193 Aveiro, Portugal
[3] - Department of Physics and CICECO – Aveiro Institute of Materials, University of Aveiro, 3810-193 Aveiro, Portugal
[4] - ITMO University, St. Petersburg 197101, Russia

ABSTRACT

We present an investigation into the magnetic sensing performance of magnetoelectric bilayered metglas / bidomain LiNbO₃ long thin bars operating in a cantilever or free vibrating regime and under quasi-static and low-frequency resonant conditions. Bidomain single crystals of Y+128°-cut LiNbO₃ were engineered by an improved diffusion annealing technique with a polarization macrodomain structure of the "head-to-head" and "tail-to-tail" type. Long composite bars with lengths of 30, 40 and 45 mm, as well as with and without attached small tip proof masses, were studied. ME coefficients as large as 550 V/cm·Oe, corresponding to a conversion ratio of 27.5 V/Oe, were obtained under resonance conditions at frequencies of the order of 100 Hz in magnetic bias fields as low as 2 Oe. Equivalent magnetic noise spectral densities down to 120 pT/Hz$^{1/2}$ at 10 Hz and to 68 pT/Hz$^{1/2}$ at a resonance frequency as low as 81 Hz were obtained for the 45 mm long cantilever bar with a tip proof mass of 1.2 g. In the same composite without any added mass the magnetic noise was shown to be as low as 37 pT/Hz$^{1/2}$ at a resonance frequency of 244 Hz and 1.2 pT/Hz$^{1/2}$ at 1335 Hz in a fixed cantilever and free vibrating regimes, respectively. A simple unidimensional dynamic model predicted the possibility to drop the low-frequency magnetic noise by more than one order of magnitude in case all the extrinsic noise sources are suppressed, especially those related to external vibrations, and the thickness ratio of the magnetic-to-piezoelectric phases is optimized. Thus, we have shown that such systems might find use in simple and sensitive room-temperature low-frequency magnetic sensors, e.g., for biomedical applications.

Keywords – Magnetic sensors, lithium niobate, bidomain crystals, magnetoelectric effect, cantilever, low frequency.

I. INTRODUCTION

Recently there has been a large demand for sensitive magnetic sensors for biomedical applications, such as magnetoencephalography and magnetocardiology, which require the ability to detect very weak fields with amplitudes lower than 10 pT and frequencies below 100 Hz [1-4]. For this purpose, a new type of magnetoelectric (ME) sensors have been intensely investigated potentially offering a sensitive, low-cost and room-temperature operation, among others [1-8]. In particular, simple magnetoelectric 2-2 laminate composites containing mechanically coupled magnetostrictive (MS) and piezoelectric (PE) layers have been shown to be capable of producing large voltages in response to weak magnetic fields [9-13]. Currently the best equivalent magnetic noise spectral density (EMND) values for ME sensors reported in the literature are of the order of 1 pT/Hz$^{1/2}$ for an operation frequency of 10 Hz [14-17]. In comparison, superconducting interference devices (SQUID), fluxgate and magnetoimpedance sensors have equivalent noise levels of the order of 1 fT/Hz$^{1/2}$, 5 pT/Hz$^{1/2}$ and 10 pT/Hz$^{1/2}$ at 10 Hz, respectively [2].

In order to achieve a high sensitivity at low frequencies, magnetic sensors should have both a large conversion factor and a low intrinsic and extrinsic noise floor. One possible approach to achieve these parameters is to use PE single crystals with large piezoelectric coefficients and very low mechanical and dielectric losses [4, 18]. Furthermore, the low-frequency fundamental bending electromechanical resonant mode of cantilever structures, where the ME effect is largely enhanced, can also be explored [1]. The intrinsic noise in ME composite sensors is mainly dominated by the thermal Johnson-Nyquist and $1/f$ noise components [4, 5]. Both of them can be minimized through the use of composites with low losses and appropriate low input noise detection circuits [19]. In principle, well designed charge or voltage amplifier schemes should yield similarly low noise floors [20, 21]. The extrinsic noise, in contrast, originates from external vibrational piezoelectric, pyroelectric and magnetic noise sources and requires more sophisticated mitigation strategies [2, 5].

Recently V. Röbisch *et al.* have developed thin-film cantilever heterostructures with layers of exchange biased magnetic amorphous alloys of FeCoSiB and PE AlN [1, 2, 20, 22]. They also introduced a frequency conversion technique for higher sensitivity at low frequencies and enhanced bandwidth of operation, having obtained an equivalent

magnetic noise level down to 60 pT/Hz$^{1/2}$ at 10 Hz. These ME systems were already successfully tested in deep brain stimulation and a real-life cardiological applications [1, 23]. Y. Wang *et al.* studied long tri-layered composites of metglas and PZT or PMN-PT multi-push-pull fibers and achieved very low noise floors of the order of 1 pT/Hz$^{1/2}$ at 10 Hz [4, 14, 16]. G. Sreenivasulu *et al.* tested long bar bi- and tri-layers of permendur and PZT, PMN-PT or langasite single-crystals and reported noise levels of the order of 10 pT/Hz$^{1/2}$ at the same frequency [24, 25]. D. Burdin *et al.* produced bi-layers of metglas, Ni or Permendur and PZT or langate single crystals and studied their nonlinear ME effect for applications in frequency conversion AC and DC magnetic field sensors [26-28].

Asymmetrical bi-layered systems with bimorph PEs, containing two oppositely poled layers along the thickness direction, are known to generate particularly large ME coefficients under bending resonant conditions [29, 30]. Furthermore, these configurations are also able to partially cancel both extrinsic vibrational and thermal noises [3, 5]. In the past, PE bimorphs have been mostly fabricated by bonding or sintering together lead-based PE plates with opposed polarizations [4, 17, 29]. Those are, however, generally associated with large interfacial mechanical losses and creep effects. Recently we have shown the possibility to produce large ME effects in composites containing lead-free LiNbO$_3$ (LNO) single-crystals [31, 32]. Furthermore, some new promising techniques have been developed to directly engineer two polarization domains in a single bulk crystal (bidomain), thus excluding any bonded interfaces [33, 34]. Among the commercially available crystal orientations the Y+128º-cut LNO approximately yields the maximum piezoelectric coefficients [31, 32]. In a previous investigation we proposed the use of square metglas / PE bi-layered composites with Y+128º-cut LNO single-crystal bidomains in sensitive magnetic sensors [35]. Here we obtained ME effects as large as 578 V/cm·Oe under bending resonance conditions at relatively high frequencies of 30 kHz and a corresponding equivalent magnetic noise spectral density of 524 fT/Hz$^{1/2}$. In the current study we continue our research of LNO-based ME bidomain composites while trying to improve their ME response, decrease the noise level and the operation frequency. To this end, composites of metglas / LNO were fabricated with the shape of long thin bars with lengths of 30, 40 and 45 mm as schematized in Fig. 1(a). The bidomain "head-to-head" (H-H) and "tail-to-tail" (T-T) structures were produced in the Y+128º-cut LNO crystals by an enhanced diffusion annealing (DA) technique [33, 34]. Fig. 1(b) shows an optical micrograph of the bidomain structure obtained in this way. The ME and magnetic noise spectral responses of the composites were then evaluated in a low-noise voltage amplifier detection circuit (see Fig. 1(c)) in two regimes: (i) fixed cantilever bars clamped at one end and (ii) free vibrating bars. In order to decrease the resonance frequency of the cantilever bars down to the order of 10 Hz, we further tested their behavior with various added tip proof masses. These studies were complemented by theoretical calculations using a simple analytical unidimensional model and a finite element method (FEM).
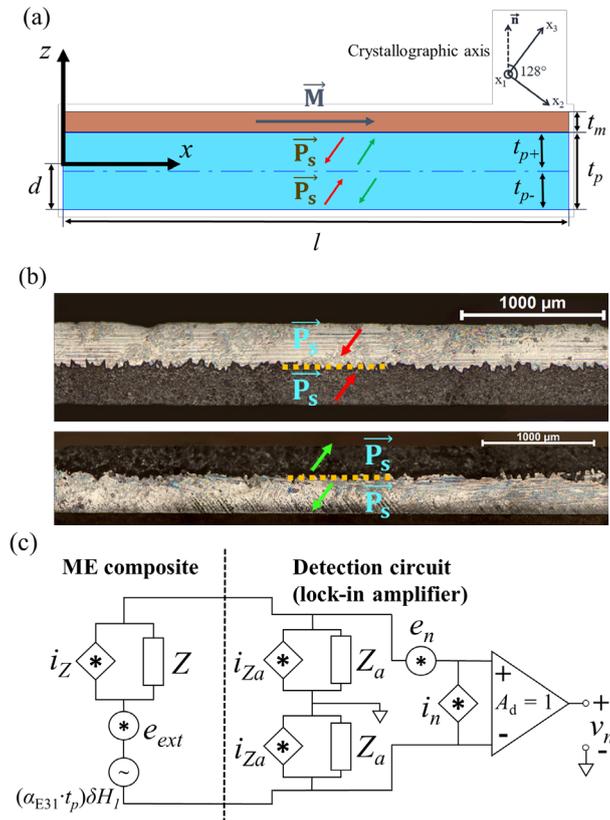
Fig. 1. (color online) (a) Scheme of the ME bi-layered long bar composite formed by a thin top MS layer and a bottom PE bidomain single crystal, where the red and green arrows represent the vectors of spontaneous polarization ($\overrightarrow{P_S}$) in the "head-to-head" (H-H) or "tail-to-tail" (T-T) domain structures, respectively. (b) Optical micrograph of the H-H and T-T bidomain configurations engineered by an improved diffusion annealing technique in selectively etched bars of Y+128º-cut LNO. (c) Equivalent circuit of the magnetic sensor including the ME composite and voltage unity gain differential amplifier detection circuit (lock-in amplifier).

II. CALCULATIONS

In this section, we use a simple analytical unidimensional dynamic model based on the linear theory of piezoelectricity and magnetostriction applied to ME composite long thin bars in order to estimate their limit ME and noise properties. As represented in Fig. 1(a), the ME composites are assumed to be ideal laminated long bars with dimensions of length (l) × width (w) × thickness (t), such that $l \gg w \gg t$, formed by a PE bidomain phase and a MS phase, perfectly bonded to each other (i.e. without any detachments or cracks). In this scheme, x_1, x_2 and x_3 are crystallographic axes and show the cut angle of the bidomain crystal, while x and z are the material axes which are directed along the length and thickness of the bar, respectively. Furthermore, d is the position of the neutral plane where the z axis is centered, t_p is the thicknesses of the PE bar (t_{p-} and t_{p+} are the thicknesses of its bottom and top domains, respectively), and t_m is the thickness of the conductive MS bar, such that $t = t_p + t_m$. The composite also has infinitely thin equipotential electrodes covering its top and bottom faces and a magnetic H field applied along its long x axis. Starting from the constitutive equations for the PE and MS phases and noting that in ideal thin bars with top and bottom electrodes and under no stress loads it is reasonable to assume null stresses everywhere except its component along the x direction (T_1) [36-39] as well as null in-plane electric fields ($E_1 = E_2 = 0$) [38, 39], we can see that, using continuum mechanics index notation, these equations can be written in the more convenient form for the PE:

$$T_1 = \overline{c_{11}^D}S_1 - \overline{h_{31}}D_3 , \qquad (1)$$
$$E_3 = -\overline{h_{31}}S_1 + \overline{\beta_{33}^S}D_3 , \qquad (2)$$

where $\overline{c_{11}^D} = \left(s_{11}^E - d_{31}^2/\varepsilon_{33}^T\right)^{-1}$, $\overline{h_{31}} = \overline{c_{11}^D}d_{31}/\varepsilon_{33}^T$ and $\overline{\beta_{33}^S} = \left(1 + \overline{h_{31}}d_{31}\right)/\varepsilon_{33}^T$, and S_1 represents the elastic strain given by $S_1 = u_{1,1}$, with u_1 being the displacement vector, T_1 – the elastic stress, D_3 – the electric displacement, and E_3 – the electric field. The material parameters here are: s_{11}^E the elastic compliance, d_{31} the PE strain coefficient, and ε_{33}^T the dielectric permittivity. For the case of the spontaneous polarization pointing in a reverse direction, the PE constants are inverted: $d_{31} \to -d_{31}$. For the MS phase we have the constitutive equation:

$$T_1 = \overline{c_{11}^H}S_1 - \overline{q_{11}}H_1 , \qquad (3)$$

where $\overline{c_{11}^H} = (s_{11}^H)^{-1}$, $\overline{q_{11}} = \overline{c_{11}^H}q_{11}$, and H_1 is the magnetic field strength. The material constants are: q_{11} the piezomagnetic coefficient (non-null in the pseudo-piezomagnetic approximation and dependent on the magnetic H bias field), and μ_{11}^T the magnetic permeability. We further assume that the highly conductive MS phase is in electrostatic ($E_3 = D_3 = 0$) and magnetostatic equilibrium (the internal magnetic field strength H_1^{int} and magnetization M_1 are homogeneous). The demagnetization effect can be taken into account through the relation $H_1^{int} = H_1 - N_1M_1$, where H_1^{int} is the fraction of the external magnetic field strength H_1 which penetrates the interior of the material, and N_1 is the effective magnetometric demagnetization factor which depends on the shape and magnetic susceptibility (χ) of the MS phase [40-43].

According to the Kirchhoff-Love theory for thin flat plates, for small deformations the displacement fields in the case of pure bending vibrations may be written in the form [36, 37] $u_1 = -z.w_{0,1}$ and $u_3 = w_0$, where w_0 is a function of the x coordinate. Some important parameters can be obtained by integration along the thickness of the composite including the resultant bending force $N_1 = \int_{-d}^{t-d} T_1 dz$, resultant shearing force $M_1 = \int_{-d}^{t-d} zT_1 dz$, averaged mass density $\langle\rho\rangle t = \int_{-d}^{t-d} \rho dz$, and voltage between electrodes $V_3 = \int_{-d}^{t_p-d} E_3 dz$ which does not depend on the x coordinate. The current flowing through the composite in the z direction can be given by $I_3 = w \int_0^l \dot{D}_3 dx$. The position of the neutral plane d is generally obtained using the equilibrium condition for the resultant force, $N_1 = 0$, when the composite is in zero applied D_3 and H_1 fields [44, 45]. From the balance laws, the unidimensional dynamical equation of motion for thin bars follows [36, 37]:

$$M_{1,11} = \langle \rho \rangle t. \ddot{w}_0 \ . \qquad (4)$$

This equation can be solved together with the constitutive relations (1-3) and some boundary conditions imposed on M_1 and w_0. Using an harmonic approximation, i.e. with all the fields having a time dependence of the type $w_0 = \delta w_0 e^{j\omega t}$, and assuming that D_3 does not depend on the z coordinate, we can thus obtain a linear expression of the form $\delta V_3 = Z\delta I_3 + (\alpha_{E31}. t_p)\delta H_1$, where $Z = 1/Y$ is the electrical impedance and α_{E31} is the voltage ME coefficient of the system. These important parameters can thus be shown to take the form:

$$Y = j\omega \frac{wl}{t_p \langle \beta_{33}^S \rangle} \left(1 + \left(\frac{t_p}{t} \right)^3 \frac{\langle h_{31} \rangle^2}{\langle \beta_{33}^S \rangle} \frac{1}{\langle c_{11}^D \rangle} f(kl) \right) ; \qquad (5)$$

$$\alpha_{E31} = -\frac{\left(\frac{t_m}{t} \right)^2 \left(\frac{t_p}{t} \right) \langle q_{11} \rangle \langle h_{31} \rangle}{\left(\frac{t_p}{t} \right)^3 \frac{\langle h_{31} \rangle^2}{\langle \beta_{33}^S \rangle} + \langle c_{11}^D \rangle (1/f(kl))} , \qquad (6)$$

where $k = \sqrt{\omega} [\langle \rho \rangle / (t^2 \langle c_{11}^D \rangle)]^{1/4}$ is the wave number, and $\langle q_{11} \rangle = (1/t_m)^2 \int_{t_p-d}^{t-d} z \overline{q_{11}} \, dz$, $\langle h_{31} \rangle = (1/t_p)^2 \int_{-d}^{t_p-d} z \overline{h_{31}} \, dz$, $\langle \beta_{33}^S \rangle = (1/t_p) \int_{-d}^{t_p-d} \overline{\beta_{33}^S} \, dz$ and $\langle c_{11}^D \rangle = (1/t)^3 \left(\int_{-d}^{t_p-d} z^2 \overline{c_{11}^D} \, dz + \int_{t_p-d}^{t-d} z^2 \overline{c_{11}^H} \, dz \right) - (t_p/t)^3 \langle h_{31} \rangle^2 / \langle \beta_{33}^S \rangle$ are thickness-independent effective flexural piezomagnetic, piezoelectric, dielectric and stiffness constants, respectively. Here, $f(kl)$ is a function of kl whose form depends on the imposed boundary conditions. A simple way to introduce mechanical friction energy losses into the model is through the use of a complex angular frequency $\omega(1 - j(1/Q))$, where Q is the mechanical quality factor [45-47]. Dielectric losses of the PE phase can also be introduced through the complex dielectric constant $\varepsilon_{33}^T(1 - j\tan(\delta))$, where $\tan(\delta)$ is the loss tangent [48]. Of note in the aforementioned expressions is the existence of certain bending electromechanical resonances, where the coefficients attain peak values. The values of these resonance frequencies, when $|Y|$ tends toward infinity, are:

$$f_{r_n} = \frac{\chi_n^2}{2\pi} \frac{t}{l^2} \sqrt{\frac{\langle c_{11}^D \rangle}{\langle \rho \rangle}}, \quad n \in \mathbb{N}, \quad (7)$$

where the χ_n constants correspond to the kl roots of the $1/f(kl)$ function. This expression shows that geometrically the bending resonance frequencies decrease linearly with decreasing thickness of the bar and inversely with increasing square of its length. Another way of dropping these frequencies is by using a large metglas-to-piezoelectric thickness ratio because of its comparatively larger density and compliance constants. Equations (5-7) show that in a simple unimorph with a large PE volume ratio, since $\langle h_{31} \rangle = \overline{h_{31}}(t_p - 2d) \approx 0$, pure bending deformations will be very weak. In PE bimorphs, on the other hand, the resonance frequencies should be minimized and the amplitude of the resonant effects maximized for opposed polarization domains with equal thicknesses, since $\langle h_{31} \rangle$ has a local maximum at $t_{p+}/t_p = 1 - d/t_p \approx 1/2$.

In the case of a free vibrating thin bar, the boundary conditions are null bending and shearing forces at both of its ends: $M_1 = 0$ and $M_{1,1} = 0$ at $x = 0$ and $x = l$. Consequently, the function in equations (5, 6) is $f(kl) = 4\sin(kl/2)\sinh(kl/2)/kl(\cos(kl/2)\sinh(kl/2) + \sin(kl/2)\cosh(kl/2))$, and the first n-th χ_n constants in (7) are ca. 4.730, 10.996, 17.279, etc. As for the case of a securely fixed cantilever bar clamped to an infinitely dense wall at the left end, the boundary conditions are a null displacement and slope at this end and a null bending and shearing forces at the other: $w_0 = 0$ and $w_{0,1} = 0$ at $x = 0$ and $M_1 = 0$ and $M_{1,1} = 0$ at $x = l$. The resultant function is thus $f(kl) = (\cos(kl)\sinh(kl) + \sin(kl)\cosh(kl))/kl(1 + \cos(kl)\cosh(kl))$, and the first n-th χ_n constants are ≈ 1.875, 4.694, 7.855, etc. These values show that the fundamental resonance mode of the fixed cantilever bar appears at a very significantly (6.4 times) lower frequency in comparison to the free bar. Also, its first overtone nearly coincides with the fundamental resonance in the free composite. Under this circumstances, we can see that, in order to achieve a fundamental resonance frequency of the order of 100 Hz in common PE materials with $\langle \rho \rangle \sim 5000$ kg/m³ and $\langle c_{11}^D \rangle \sim c_{11}^D/12 \sim 1.5 \times 10^{10}$ N/m², one should have a long cantilever with a length square to thickness ratio of $l^2/t \sim 10$ m.

Fig. 1(c) shows the differential voltage amplifier equivalent circuit of the ME magnetic field sensor used in this study. It consists of the ME composite, with its internal impedance and intrinsic current (i_z) and extrinsic voltage noise sources (e_{ext}), as well as a unity gain differential amplifier (lock-in) and its characteristic input impedance ($2Z_a$), current (i_n) and voltage (e_n) noise spectral densities. The extrinsic noise here includes all external sources, mainly the

acoustic and vibrational, thermal and magnetic ones [2]. Since the composite behaves essentially as a high-impedance capacitor, we can assume that the intrinsic noise is dominated by the thermal Jonhson-Nyquist noise with a RMS current noise spectral density of $i_Z = \sqrt{4k_B T Y'}$ [49, 50], where k_B is the Boltzmann constant, T is the temperature, and Y' and Y'' are the real and imaginary parts of the composite's admittance, respectively. The total RMS voltage noise spectral density, in units of V/Hz$^{1/2}$, at the output of this detection circuit is thus:

$$v_n = \sqrt{4k_B T Z'_{eq} + |Z_{eq}|^2 i_n^2 + e_n^2 + |Z_{eq}/Z|^2 e_{ext}^2} , \qquad (8)$$

where Z_{eq} is the equivalent impedance of the circuit equal to $Z \| 2Z_a$. The equivalent EMND which evaluates the detection limit in the circuit in units of T/Hz$^{1/2}$, is then EMND $= v_n / |\delta V_{ME}/\delta H|$, where $\delta V_{ME}/\delta H = |Z_{eq}/Z|(\alpha_{E31}.t_p)$ is the voltage per magnetic amplitude of the signal due to the ME effect measured at its output. In the thin bars this coefficient can be estimated using equations (6) and (8). Considering only the intrinsic thermal noise sources yields a magnetic noise density approximately proportional to $\sqrt{(1/twl)(1/f)\tan(\delta)}$ at low frequencies and $\sqrt{(l/t^2 w)(1/Q)}$ under resonance conditions. This shows that, in order to minimize the noise in a composite with a given resonance frequency, one has to increase its volume and use phases with a large Q and small $\tan(\delta)$ factor, which is generally the case in single crystals. The signal-to-noise ratio for this sensor is related to the EMND by the expression SNR $= \left(\delta V_{ME\,RMS}/v_n \sqrt{\Delta f}\right)^2 = (1/\text{EMND})^2 \left(\delta H_{RMS}/\sqrt{\Delta f}\right)^2$, where Δf is the bandwidth of the input filter of the amplifier.

Using equations (5-8) and values of the material constants obtained from the literature, we can estimate the impedance, magnetoelectric coefficient, intrinsic voltage noise density and intrinsic magnetic noise density for some metglas / bidomain Y+128º-cut LNO free and side-fixed long bars with different lengths (l = 30, 40 and 45 mm). The bars also have a width of w = 5 mm and thicknesses of t_m = 29 μm for the metglas phase, and t_p = 0.5 mm for the LNO phase with equally sized domains ($t_{p-} = t_{p+} = t_p/2$). Typical values of $\tan(\delta)$ = 2% and Q = 250 were set, as well as a room temperature of T = 300 K. The material constants used for the Y+128º-cut LNO crystal, with the x_1 crystallographic direction along the width of the bar, were $\varepsilon_{33}^T/\varepsilon_0$ = 49.83, d_{31} = − 27.24 pC/N, $s_{11}^E = 6.91 \times 10^{-12}$ m²/N and ρ = 4647 kg/m³ [51]. The constants for the isotropic metglas alloy were: $s_{11}^H = 10 \times 10^{-12}$ m²/N and ρ = 7900 kg/m³ [52-54]. According to the data found in the literature, the intrinsic piezomagnetic coefficient for metglas can be as large as q_{11}^{int} = 4 ppm/Oe for a bias field roughly of the order of 1 Oe [43, 55-59], where the differential magnetic susceptibility is of the order of χ = 1000 [52, 56-58]. Consequently, taking the demagnetization effect into account, the effective piezomagnetic constant can be given by [40, 41, 43] $q_{11} = q_{11}^{int}/(1 + N_1\chi)$. Using the tabulated magnetometric demagnetization factors for rectangular prisms calculated in the literature [60], we interpolated their values for the aspect ratio of our MS layers having obtained N_1 = 5.6725 x 10⁻⁴, 3.9621 x 10⁻⁴ and 3.4316 x 10⁻⁴ for increasing length of the bars. These values are rather close to the ones calculated for an ellipsoid with equivalent principal axes using the well-known analytic expression [61]. This shows that, as the length of the bars increases, the magnetic field penetrates them more easily resulting in an increase of the maximum piezomagnetic coefficient and a decrease of the bias field at which it is attained. The resultant thickness averaged constants in the model are thus: $\langle \rho \rangle$ = 4825 kg/m³, $\langle c_{11}^D \rangle$ = 1.23 x 10¹⁰ N/m², $\langle h_{31} \rangle$ = 2.95 x 10⁹ V/m, $\langle \beta_{33}^S \rangle$ = 2.99 x 10⁹ m/F and $\langle q_{11}^{int} \rangle$ = 3.54 x 10⁶ N/(m².Oe). An ideal detection circuit with $Z_a = \infty$, $i_n = 0$ and $e_n = 0$ as well as no external noise sources ($e_{ext} = 0$) were assumed. The results of this calculations are shown in Fig. 2. From them we can see that the absolute impedance ($|Z|$) initially decreases with the frequency as $1/f$, while the thermal noise density (e_Z) and equivalent magnetic noise density (EMND) decrease with $1/\sqrt{f}$ and the ME coefficient (α_{E31}) is constant. The impedance evidences a minimum at the frequency of resonance closely followed by a maximum at a frequency of antiresonance. The ME coefficient and voltage noise are maximized at this last frequency. The EMND shows a very desirable wide minimum between these two frequencies where it can drop by up to an order of magnitude. It subsequently increases up to a maximum at ca. 1.5 times this frequency, where the ME effect is minimized. The calculated resonance frequencies for the free cantilever long bars with increasing lengths are shown to be as low as 525, 296 and 234 Hz, respectively. Disregarding the demagnetization effect, the corresponding minimum EMND should increase with the length as 1.04, 1.20 and 1.28 pT/Hz$^{1/2}$. The resonance frequencies of the free bars with the same lengths are comparatively larger at 3344, 1881 and 1486 Hz and, ignoring the demagnetization effect, should have smaller corresponding EMND of 0.39, 0.45 and 0.48 pT/Hz$^{1/2}$. Taking the demagnetization effect into account results in ca. 30% smaller ME effects which increase with the length of the bar, as pictured, and thus in larger minimum EMND values of 1.67 pT/Hz$^{1/2}$ for the cantilever bars and 0.63 pT/Hz$^{1/2}$ for the free bars which change only very slightly with the lengths. Lastly, we note that the thickness ratio

between phases of $t_p/t \sim 0.95$ used in this calculations is far from optimum. Thus, e.g. in the case of the 45 mm long cantilever bar with a constant thickness the resonant ME effect can be shown to be increased by more than three times and the corresponding EMND to be decreased down to less than 0.5 pT/Hz$^{1/2}$ for a thickness ratio of the PE phase t_p/t between 0.7 and 0.2. Figs. 2(c) and 2(d) show the characteristic displacement of the 45 mm long bidomain PE crystals operating under their fundamental electromechanical bending resonant modes obtained using a tridimensional finite element method (FEM) in COMSOL Multiphysics.
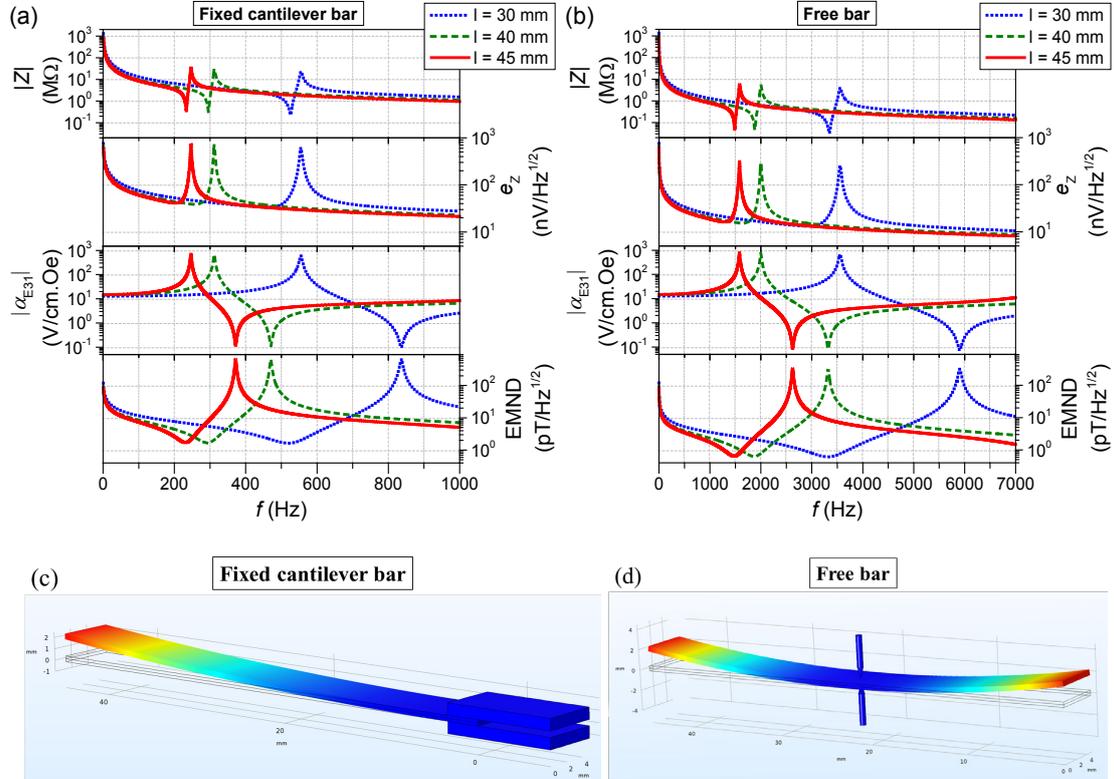

Fig. 2. (color online) Calculated spectrum of the absolute impedance ($|Z|$), intrinsic thermal noise density (e_Z), absolute ME coefficient ($|\alpha_{E31}|$) and intrinsic equivalent magnetic noise density (EMND) of long thin bar composites (with length l = 30, 40 and 45 mm and width w = 5 mm) of metglas (29 μm thick) and a Y+128°-cut symmetric bidomain LNO crystal (0.5 mm thick) operating in a: (a) fixed cantilever and (b) free vibrating regime. FEM simulated fundamental bending electromechanical resonance mode of the 45 mm long bidomain PE crystals operating in a (c) fixed cantilever and (d) free vibrating regime.

III. EXPERIMENTAL

Two ferroelectric macrodomains with inverted spontaneous polarizations and equal thicknesses were engineered in commercial congruent LNO Y+128°-cut single-crystalline wafers (ELAN Company Ltd.) using an improved diffusion annealing (DA) technique [33, 34]. In it, a directed diffusion of Li$_2$O is promoted during high-temperature annealing in such a way that one of the domains is gradually reversed from the surface to the bulk under the influence of an internal electric field [30, 62]. For thermodynamic reasons there is always a small rough interdomain region in the bidomain crystals that negatively influences its quality. We estimated that the interdomain region had a thickness of less than 45 μm in every studied sample. Three LNO long bars were cut, with the x_1 crystallographic direction along the width of the bar, having different lengths of l = 30 mm (with a "tail-to-tail" T-T polarization), 40 mm and 45 mm (both with a "head-to-head" H-H polarization). Their thickness was of t_p = 0.5 mm and width of w = 5 mm. Asymmetrical ME composites were subsequently prepared by bonding a single layer of commercial 2826MB type (Fe$_{0.4-0.5}$Ni$_{0.4-0.5}$Mo$_{0.05-0.1}$B$_{0.01-0.05}$) metglas foil (Hitachi Metals Europe GmbH), with a thickness of t_m = 29 μm, to the top of the LNO bars with equal widths and lengths. The bonding was achieved using an epoxy adhesive (Devcon epoxy 14260) which was subsequently cured at 50°C for 3 hours under an applied vertical pressure of 100 kPa by a piston cylinder. The bottom faces of the PE crystals were painted with a silver paste.

yered samples at room temperature in two regimes: (i) securely fixed cantilever bars clamped at one end (Fig. 2(c)) and (ii) free vibrating bars (Fig. 2(d)). In the former case, one end side of the ME composites were strongly clamped between two brass plates, with a large Young modulus and density, which were fixed to a large mass so that it's vibration was guaranteed to be very low and the displacement of the bar at this end to be null. In the latter case, the samples were fixed by their middle points by means of two weak spring-loaded bronze contacts. The 3D models of the samples and fixation methods are presented in Figs. 2(c) and 2(d). With the intent of further decreasing the bending resonance frequencies of the ME composites, we added small proof masses of $m = 0.1$, 0.6 and 1.2 g to the free tip of the 45 mm long cantilever bar.Dynamic ME and electrical measurements were performed in the range from $f = 1$ Hz up to 100 kHz on the bila

The impedance, voltage noise density and direct ME effect for the samples were measured using a high input impedance and low input noise lock-in differential amplifier (Zurich Instruments®, MFLI). A home-made setup was used in the ME measurements consisting of two collinear Helmholtz coils which produced a small amplitude modulated AC (δH) and DC bias (H) highly homogeneous magnetic fields across the complete volume of the samples [31]. The samples were connected to the detection circuit using a triaxial cable with a grounded outer electromagnetic shield. In the sensitive noise measurements the samples together with the support were placed inside a grounded metglas-coated and damped aluminum box, thus partially shielded against environmental electromagnetic fields and external vibrations. The signal from the composites was measured by the lock-in operating in its lowest 1 mV input range, as a function of the frequency and with the 3 dB bandwidth of the input filter set to 0.01 times this frequency, without any applied AC magnetic field, using the noise-measuring mode of the device. The obtained results were expressed in terms of the voltage noise spectral density which corresponds to the root mean square of the measured voltage amplitude normalized by the square root of the bandwidth of the input filter in units of V/Hz$^{1/2}$. The EMND of the system was finally calculated from it's measured ME signal and noise density.

IV.RESULTS AND DISCUSSION

The measured impedance spectra of the long thin bar ME composites with different lengths and operating in a (i) fixed cantilever or (ii) free vibrating regime are depicted in Fig. 3. They evidence a series of resonance and antiresonance peaks associated with low-frequency bending electromechanical modes which have a good correspondence with the ones obtained in the unidimensional calculations. Various informative parameters can be extracted from these spectra, including the low-frequency capacitance (C) and dielectric loss tangent ($\tan(\delta)$) obtained at 100 Hz, resonance frequencies (f_r and f_a), as well as effective electromechanical coupling (k_{eff}) and mechanical quality (Q) factors of the fundamental resonance. Those are summarized in Table 1. The values of capacitance in the samples are of the order of 100 pF and increase with their length as predicted by the expression $C = \varepsilon_{33}^T wl/t_p$. The dielectric loss tangents are shown to be quite low at only $\tan(\delta) \sim 2\%$. The effective electromechanical coupling factors are $k_{eff} \sim 0.2$ in all samples, being significantly lower than the 0.33 from the calculations, which can indicate smaller than expected piezoelectric constants. The mechanical quality factors, calculated as the ratio between the resonance frequency and full width at half maximum of the admittance Y' peaks, take values of $Q \sim 300$ in the bars with $l = 40$ mm and 45 mm and with a H-H bidomain structure. These values are still relatively high taking into account that they include the friction losses introduced by internal defects produced during the DA treatment and a significantly thick (ca. 10 μm) intermediate layer of viscous epoxy. The composite with $l = 30$ mm and a T-T structure exhibits a two times smaller quality factor, possibly due to a local broadening of the interdomain region that was not detected by initial testing. The quality factors also tend to be slightly smaller in the fixed cantilever regime indicating an imperfect non-vibrating tight fixation at the end of the bars.
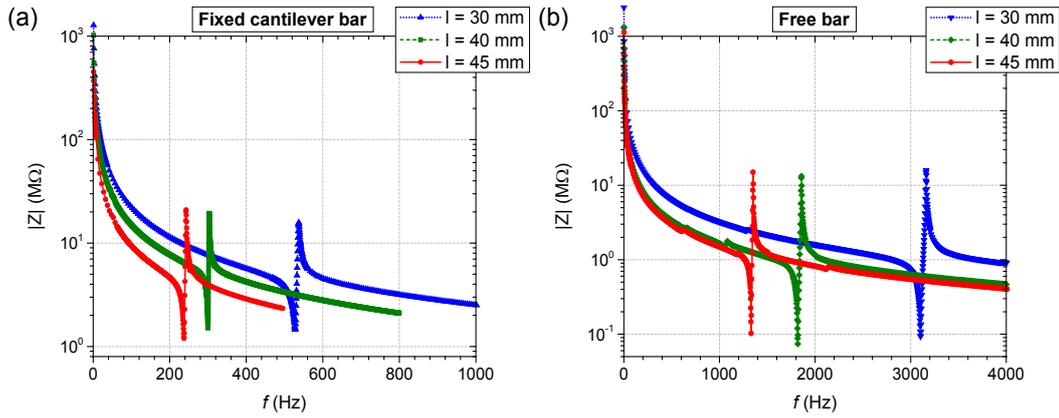
Fig. 3. (color online) Impedance spectra of the long thin bar metglas / bidomain LNO composites (with length l = 30, 40 and 45 mm) operating in a: (a) fixed cantilever and (b) free vibrating regime.

The results of the quasi-static ME measurements in the long bar composites, performed with a modulated field with an amplitude of δH = 0.5 Oe and frequency of f = 10 Hz, as a function of the H bias field applied in the x direction, are presented in Fig. 4. These curves closely follow the piezomagnetic constant of the metglas phase, $q = \partial S/\partial H$. The maximum ME coefficients are shown to be as large as α_{E31} = 7.2 V/cm·Oe in the cantilever 45 mm long bar under a bias field of only 2 Oe at such a low frequency. In general, we see an increase of the maximum ME coefficient with increasing length of the bar, as well as a decrease in the bias field at which this maximum is attained. This behavior can be attributed to the larger volume of the metglas phase and improved aspect ratio which thus tends to reduce the demagnetization [40-42, 63] and shear lag effects [64, 65], resulting in an effective enhancement of the piezomagnetic coefficients. The ME effect is slightly larger in the fixed cantilever scheme when compared to the free vibrating one, possibly because of the closer proximity of it's first resonant mode. The measured quasi-static output voltage amplitude (δV_{ME}) as a function of the field modulation amplitude (δH) for the 45 mm long bars, with a fixed optimum bias of H = 2 Oe, is shown in the inset of Fig. 4. From here we see that the composite has a very linear response for fields of up to at least δH = 0.5 Oe.
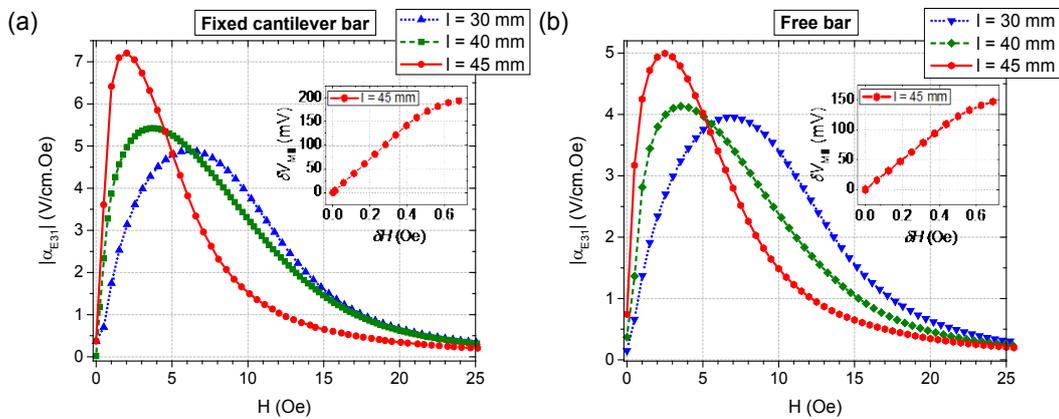

Fig. 4. (color online) Quasi-static in-plane direct ME coefficients ($|\alpha_{E31}|$) measured as a function of the magnetic H bias field (with f = 10 Hz and δH = 0.5 Oe) in the long thin bar metglas / bidomain LNO composites (with length l = 30, 40 and 45 mm) operating in a: (a) fixed cantilever and (b) free vibrating regime. The insets show the measured voltage amplitude (δV_{ME}) as a function of the field modulation amplitude (δH) in the 45 mm long bars (with f = 10 Hz and H = 2 Oe).

Fig. 5 shows the transversal ME coefficients measured in the dynamic regime as a function of the frequency of the modulated field with an amplitude of δH = 0.05 Oe and an applied H bias field corresponding to the maximum ME effect as measured in the quasi-static regime. The coefficients exhibit large peaks proportional to the mechanical Q factor at frequencies corresponding to the antiresonance frequency in the impedance spectra, where the bending displacement is very large whenever the current is null. Once again, we can see that the quality factors are ca. twice as large in the H-H 45 mm and 40 mm long bars as compared to the T-T 30 mm long one. The large ME coefficients with an increasing length of the bars are respectively 147, 395 and 440 V/cm·Oe at resonance in the cantilever mode, and the

same tendency is observed in the free vibrating mode 179, 443 and 478 V/cm·Oe. Even so, the measured ME effects are shown to be almost two times smaller than the ones predicted in the calculations section. This deviation can be attributed to additional losses in the transference of strain between phases due to the rough intermediate epoxy layer [40, 41, 66], smaller effective piezoelectric constants because of an incomplete polarization, and the complex dependence of the magnetostrictive effect on the magnetic field and stress [67]. The slightly smaller effects observed in the fixed cantilevers in relation to the free bars are likely due to an imperfect end fixing of the bar and, thus, a transference of part of its vibration to the clamp support where the stress is maximized. We note that the amplitude and frequency of these resonant modes are very sensitive to the configuration of the sample support, especially in the cantilever mode. The ME effects also tend to decrease at frequencies below ca. 10 Hz, which is related to the finite impedance of the input circuit and composites.
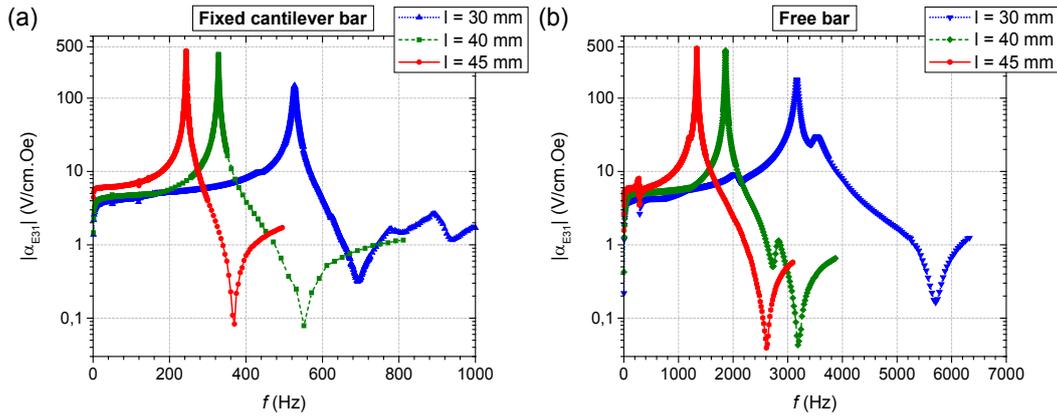

Fig. 5. (color online) Dynamic direct ME coefficients ($|\alpha_{E31}|$) measured as a function of the field modulation frequency (with optimal bias fields of respectively H = 6.5, 3.5 or 2 Oe, for each length, and δH = 0.05 Oe) in the long thin bar metglas / bidomain LNO composites (with length l = 30, 40 and 45 mm) operating in a: (a) fixed cantilever and (b) free vibrating regime.

The voltage noise spectral densities of the detection circuits and ME samples were measured without application of modulated magnetic field and in an environment partially shielded from external stray vibrations and electromagnetic fields. The results of these measurements are shown in Fig. 6 including those for a non-PE and non-MS reference 100 pF capacitor connected to the input of the lock-in amplifier. In general, this reference measurement shows a typical frequency dependence of the voltage noise density having a dominant $1/f$ component for frequencies between ca. 100 Hz and 10 kHz and a constant level of ca. 340 nV/Hz$^{1/2}$ below 100 Hz which closely follows the thermal Jonhson-Nyquist noise associated with the input impedance of the device ($\sqrt{4k_BTZ'_{eq}}$), where Z_{eq} = 100 pF‖2Z_a, and the input impedance of the lock-in is Z_a = 10 MΩ‖40 pF. This dependence is followed at $f > 10$ kHz by a constant noise ground level of ca. 1.6 nV/Hz$^{1/2}$ associated with the input voltage noise density e_n of the amplifier. The contributions of the input current noise of the detection circuit ($|Z_{eq}|i_n$) and extrinsic voltage noise sources ($|Z_{eq}/Z|e_{ext}$) to the total noise, as presented in equation (8), are not apparent in the entire frequency range of this reference measurement. The results of the noise measurements performed with the ME samples are shown to be relatively similar to the measurements in the reference capacitor with the exception of some additional resonance peaks at certain frequencies. This proves that off resonance the noise of the magnetic sensors is mostly dominated by the input noise of the detection circuit. Superimposed on the figures are the calculated thermal Jonhson-Nyquist noise components ($\sqrt{4k_BTZ'_{eq}}$) for the sensors with the 45 mm long bars using the unidimensional model. From here we can see that this noise source is mostly responsible for the noise peaks observed under antiresonance conditions in the long bar measurements and part of the remaining spectrum. The noise peaks associated with the bending resonance modes of the free bars and higher harmonic modes of the cantilever bars observed above 1 kHz have amplitudes close to the ones due to the thermal noise, as predicted by the model. The fundamental resonance modes of the cantilever bars measured at lower frequencies, on the other hand, exhibit amplitudes more than one order of magnitude larger than the calculated values. This suggests that in this range the noise level is dominated by its $|Z_{eq}/Z|e_{ext}$ component related to external noise sources. This external noise dependence might have arisen mainly from environmental vibrations because of the cantilever's high susceptibility to low-frequency movements of its clamp support and the high difficulty in insulating the ME system against them, including the ones originating from the operating lock-in itself. The free bars also appear to pick up some of this extrinsic noise mainly in the frequency range between 100 Hz and 1 kHz. In summary, the resonance peak

voltage noise densities measured in this part for increasing length of the bars were ca. 1810, 7240 and 9200 nV/Hz$^{1/2}$ in the cantilever case, and 44, 184 and 289 nV/Hz$^{1/2}$ in the free bar case.
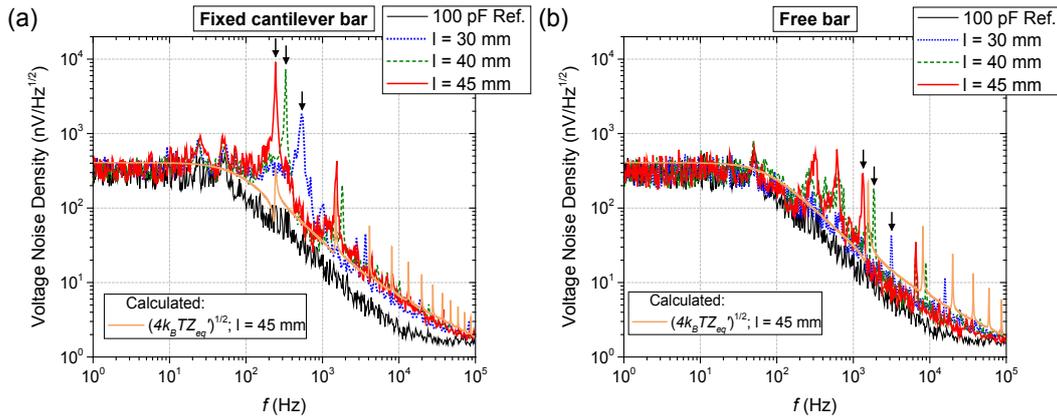

Fig. 6. (color online) Voltage noise spectral density measured as a function of the frequency in the long thin bar metglas / bidomain LNO composites (with length $l = 30$, 40 and 45 mm) operating in a: (a) fixed cantilever and (b) free vibrating regime. The black arrows point out the fundamental bending electromechanical resonant modes. Superimposed are the results of the measured input voltage noise of the lock-in amplifier connected to a reference 100 pF capacitor and calculated impedance thermal Jonhson-Nyquist noise ($\sqrt{4k_BTZ'_{eq}}$) for the sensor with the 45 mm long bar using the unidimensional model.

The most important figure of merit of a magnetic sensor is the equivalent magnetic noise density which quantifies its lower detection limit. This value can be calculated from the output voltage noise density (v_n) and ME coefficient (α_{E31}) of the circuit as EMND $= v_n/|\delta V_{ME}/\delta H|$, where $\delta V_{ME}/\delta H = |Z_{eq}/Z|(\alpha_{E31}.t_p)$. The frequency dependence of the EMND for our ME composites is shown in Fig. 7. Superimposed are the results of the calculated EMND for the long bars and detection circuits using the unidimensional model and taking into account only the impedance thermal Jonhson-Nyquist noise component. As in the case of the voltage noise, the magnetic noise is shown to exhibit nearly a constant behavior at frequencies below 100 Hz taking values of the order of 180 pT/Hz$^{1/2}$. As predicted in the calculations section, we observe the presence of relatively wide minima around the resonance frequencies. Furthermore, the amplitude of these minima also tends to increase with the square root of the length of the bars. The results of the calculations are especially accurate in the case of the free vibrating bars with higher frequency resonant modes, where the intrinsic thermal noise appears to be the dominant factor. In the free bar with a length of 45 mm the measured noise is as low as 1.2 pT/Hz$^{1/2}$ at a resonance frequency of 1335 Hz. In the fixed cantilever bars with lower resonant frequencies, the limit of detection peak is sharper and one order of magnitude higher than predicted due to additional noise introduced by the environment. Even so, for the bar with a length of 45 mm the measured magnetic noise is still quite respectable at only 37 pT/Hz$^{1/2}$ for a resonance frequency of 243.6 Hz. The most important results for the ME composite bars obtained in this part are summarized in Table 1.
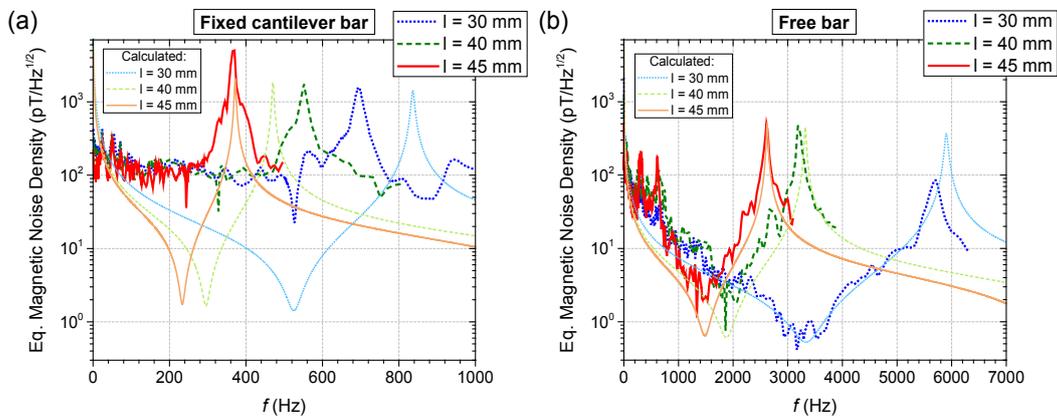

Fig. 7. (color online) Equivalent magnetic noise spectral density (EMND) measured as a function of the frequency in the long thin bar metglas / bidomain LNO composites (with length $l = 30$, 40 and 45 mm) operating in a: (a) fixed cantilever and (b) free vibrating regime. Superimposed are the results of the calculated EMND for the sensors with the

long bars using the unidimensional model and taking into account only the impedance thermal Jonhson-Nyquist noise component.

TABLE 1. Summary of experimentally obtained ME and noise properties of the metglas / LNO bilayered long bars. Here, C and $\tan(\delta)$ are the low-frequency (100 Hz) parallel capacitance and loss tangent, f_r and f_a are the resonance and antiresonance frequencies of the fundamental electromechanical bending mode, k_{eff} is the effective electromechanical coupling factor ($k_{eff}^2 = (f_a^2 - f_r^2)/f_a^2$), Q is the mechanical quality factor, $|Z(f_a)|$ is the peak impedance amplitude in antiresonance, $|\alpha_{E31}|$ are the ME coefficients measured under quasi-static (at 10 Hz) and resonant conditions (at f_a), and EMND is the corresponding equivalent magnetic noise spectral density.

Sample	l = 45 mm		l = 40 mm		l = 30 mm	
	fixed	free	fixed	free	fixed	free
C, pF	129		106		71	
$\tan(\delta)$, %	2.6		2.0		1.9	
f_r, Hz	237.5	1307	322.0	1822	518.0	3108
f_a, Hz	243.6	1335	328.3	1860	527.0	3166
k_{eff}	0.222	0.204	0.195	0.201	0.184	0.191
Q	253	280	295	305	129	146
$|Z(f_a)|$, MΩ	20.9	14.9	19.4	13.2	15.7	15.9
$|\alpha_{E31}(10\,\text{Hz})|$, V/cm·Oe	7.2	5.0	5.4	4.1	4.9	4.0
$|\alpha_{E31}(f_a)|$, V/cm·Oe	440	478	395	443	147	179
EMND(10 Hz), pT/Hz$^{1/2}$	126	181	168	221	185	227
EMND(f_a), pT/Hz$^{1/2}$	37	1.2	32.0	0.8	23	0.4

In order to further suppress the resonance frequency of the magnetic sensing element, we added small proof masses to the free tip of the 45 mm long fixed cantilever. Fig. 8 shows the results of this measurements performed with added masses of m = 0.1, 0.6 and 1.2 g. We can see a progressive decrease of the bending resonance frequency from 243.6 Hz of the simple cantilever down to 177.8, 109.8 and 80.8 Hz. The peak ME coefficients under resonant conditions also exhibit a small enhancement and tend to slightly decrease with larger masses as 549.6, 493.4 and 468.5 V/cm·Oe. Furthermore, the width of the peaks also tends to decrease. Like before, the voltage noise measurements evidence the presence of peaks at the antiresonance frequencies, mostly associated with external noise sources and the impedance thermal noise. These peaks also increase as the frequency of resonance becomes lower. As a result, the obtained equivalent magnetic noise densities shown in Fig. 8(c) initially slightly decrease with the frequency until achieving a sharp minimum at resonance, and subsequently rapidly increase. These minima with decreasing resonance frequency are respectively equal to 46, 53 and 68 pT/Hz$^{1/2}$. Thus, in summary, by using a fixed cantilever metglas / LNO 45 mm long bar with an added tip mass of 1.2 g we managed to decrease its fundamental bending resonance frequency down to only 81 Hz, where the equivalent magnetic noise density can be as low as 68 pT/Hz$^{1/2}$. This value is, however, quite large when compared to the noise density of ca. 120 pT/Hz$^{1/2}$ obtained for the same cantilever operating at a smaller non-resonant frequency of 10 Hz. From a practical point of view, the bandwidth of the noise minimum is also very small. Hence, in order to make full use of the enhanced sensitivity under these low-frequency resonant conditions, it is imperative to decrease the level of the noise introduced by external sources and the detection circuit down to the level of the intrinsic noise (as shown in the calculations section), where it can be as low as 2 pT/Hz$^{1/2}$.
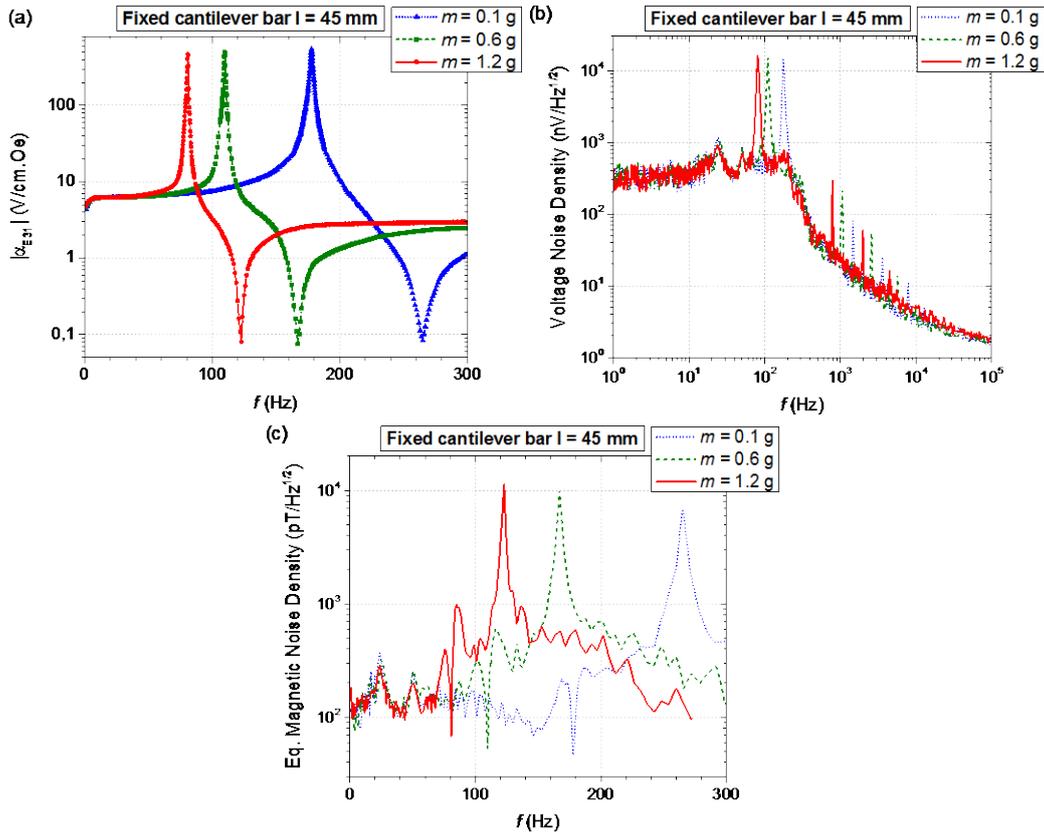
Fig. 8. (color online) (a) Dynamic ME coefficient (with $H = 2$ Oe and $\delta H = 0.05$ Oe), (b) voltage noise spectral density and (c) EMND measured as a function of the frequency in the metglas/bidomain LNO fixed cantilever composite with length $l = 45$ mm and proof tip masses of $m = 0.1$, 0.6 and 1.2 g.

V. CONCLUSIONS

We have evaluated the magnetic sensing performance of metglas / Y+128°-cut bidomain LNO ME long thin bars operating in a cantilever and free vibrating regimes and under quasi-static and resonant conditions. ME coefficients as large as 550 V/cm·Oe, corresponding to a conversion ratio of 27.5 V/Oe, were obtained under resonance conditions at frequencies of the order of 100 Hz in bias fields as low as 2 Oe. An equivalent magnetic noise density down to 120 $pT/Hz^{1/2}$ at 10 Hz and 68 $pT/Hz^{1/2}$ at a resonance frequency as low as 81 Hz was measured in a 45 mm long cantilever bar with a tip proof mass of 1.2 g. In the same sample without any added tip mass, the magnetic noise was shown to be as low as 37 $pT/Hz^{1/2}$ at a resonance frequency of 244 Hz and 1.2 $pT/Hz^{1/2}$ at 1335 Hz in a fixed cantilever and free vibrating regime, respectively. These systems are therefore competitive in comparison to some recently developed ME cantilever sensors with minimum magnetic noises of ca. 1 $pT/Hz^{1/2}$ under resonance at ca. 1 kHz and 60 $pT/Hz^{1/2}$ at 10 Hz using a frequency conversion technique [1, 2]. We note that a simple unidimensional dynamic model further predicted the possibility to drop the 37 $pT/Hz^{1/2}$ value down to at least 2 $pT/Hz^{1/2}$ in case all the extrinsic noise sources are removed, especially those related to external vibrations. An optimization of the thickness ratio of the magnetic-to-piezoelectric phases is further expected to reduce this value by a factor of three.

Due to its low magnetic noise and resonance frequencies, we expect the bidomain LNO cantilever technology to find future applications in magnetic and current sensing, for example, in biomedical areas such as magnetocardiography or magnetoencephalography, eventually replacing sensors based on the giant magnetoresistance (GMR) or Hall effect. The advantages of these systems include a passive room temperature operation, low mechanical losses in the bidomain against bimorph, much higher thermal and chemical stability of LNO crystals in opposition to PZT / PMN-PT, non-hysteretic PE effect, large resistance to creep and ageing effects, lead-free nature and simple and cheap fabrication process. Its drawbacks at this point are, however, a relatively large size, need for a magnetic bias field and a high sensitivity to vibrations. Numerous strategies have already been developed in the literature in order to overcome these problems, such as the integration of a bias field into self-biased ME heterostructures [1] and a gradiometer [68] or tuning fork structure [69] with two identical ME cantilevers, where the common mode vibrational noise can be cancelled. Future developments in this systems should be directed toward further increasing the ME coefficient, reducing the detection circuit noise, decreasing the resonance frequency and increasing the operation bandwidth. These

shall therefore include: increasing the thickness ratio of the MS / PE phases, improving the bonding / deposition technology, employing higher input impedance and lower input noise detection circuits, optimizing the poling by the diffusion annealing technique and developing an array structure to increase the sensitivity and suppress the external noise.

ACKNOWLEDGMENTS

REFERENCES

[1] V. Röbisch, S. Salzer, N. O. Urs, J. Reermann, E. Yarar, A. Piorra, C. Kirchhof, E. Lage, M. Höft, G. U. Schmidt, R. Knöchel, J. McCord, E. Quandt, D. Meyners, "Pushing the detection limit of thin film magnetoelectric heterostructures", *J. Mater. Res.*, **32**(6), 1009-1019, (2017). http://dx.doi.org/10.1557/jmr.2017.58

[2] S. Salzer, V. Röbisch, M. Klug, P. Durdaut, J. McCord, D. Meyners, J. Reermann, M. Höft, R. Knöchel, "Noise Limits in Thin-Film Magnetoelectric Sensors With Magnetic Frequency Conversion", *IEEE Sens. J.*, **18**(2), 596-604, (2018). http://dx.doi.org/10.1109/JSEN.2017.2776039

[3] J. Zhai, Z. Xing, S. Dong, J. Li, D. Viehland, "Detection of pico-Tesla magnetic fields using magneto-electric sensors at room temperature", *Appl. Phys. Lett.*, **88**(6), 062510-062512, (2006). http://dx.doi.org/10.1063/1.2172706

[4] Y. J. Wang, J. Q. Gao, M. H. Li, Y. Shen, D. Hasanyan, J. F. Li, D. Viehland, "A review on equivalent magnetic noise of magnetoelectric laminate sensors", *Phil. Trans. R. Soc. A*, **372**(2009), 20120455-20120467, (2014). http://dx.doi.org/10.1098/rsta.2012.0455

[5] Z. Xing, J. Zhai, J. Li, D. Viehland, "Investigation of external noise and its rejection in magnetoelectric sensor design", *J. Appl. Phys.*, **106**(2), 024512-024519, (2009). http://dx.doi.org/10.1063/1.3176500

[6] D. T. H. Giang, P. A. Duc, N. T. Ngoc, N. H. Duc, "Geomagnetic sensors based on Metglas/PZT laminates", *Sens. Actuators A-Phys.*, **179** 78-82, (2012). http://dx.doi.org/https://doi.org/10.1016/j.sna.2012.03.030

[7] N. H. Duc, B. D. Tu, N. T. Ngoc, V. D. Lap, D. T. H. Giang, "Metglas/PZT-Magnetoelectric 2-D Geomagnetic Device for Computing Precise Angular Position", *IEEE Trans. Magn.*, **49**(8), 4839-4842, (2013). http://dx.doi.org/10.1109/TMAG.2013.2241446

[8] L. Bian, Y. Wen, P. Li, Y. Wu, X. Zhang, M. Li, "Magnetostrictive stress induced frequency shift in resonator for magnetic field sensor", *Sens. Actuators A-Phys.*, **247** 453-458, (2016). http://dx.doi.org/https://doi.org/10.1016/j.sna.2016.06.041

[9] M. Fiebig, "Revival of the magnetoelectric effect", *J. Phys. D: Appl. Phys.*, **38**(8), R123-R152, (2005). http://dx.doi.org/10.1088/0022-3727/38/8/R01

[10] C.-W. Nan, M. I. Bichurin, S. Dong, D. Viehland, G. Srinivasan, "Multiferroic magnetoelectric composites: Historical perspective, status, and future directions", *J. Appl. Phys.*, **103**(3), 031101-031135, (2008). http://dx.doi.org/10.1063/1.2836410

[11] H. Palneedi, V. Annapureddy, S. Priya, J. Ryu, "Status and Perspectives of Multiferroic Magnetoelectric Composite Materials and Applications", *Actuators*, **5**(1), 9-39, (2016). http://dx.doi.org/10.3390/act5010009

[12] J. Ma, J. Hu, Z. Li, C.-W. Nan, "Recent Progress in Multiferroic Magnetoelectric Composites: from Bulk to Thin Films", *Adv. Mater.*, **23**(9), 1062-1087, (2011). http://dx.doi.org/10.1002/adma.201003636

[13] G. Srinivasan, "Magnetoelectric Composites", *Annu. Rev. Mater. Res.*, **40** 153-178, (2010). http://dx.doi.org/10.1146/annurev-matsci-070909-104459

[14] Y. Wang, M. Li, D. Hasanyan, J. Gao, J. Li, D. Viehland, "Geometry-induced magnetoelectric effect enhancement and noise floor reduction in Metglas/piezofiber sensors", *Appl. Phys. Lett.*, **101**(9), 092905-092908, (2012). http://dx.doi.org/10.1063/1.4737906

[15] F. Cong, J. Jie, M. Jiashuai, L. Di, X. Haiqing, Z. Xiangyong, L. Haosu, "Significant reduction of equivalent magnetic noise by in-plane series connection in magnetoelectric Metglas/Mn-doped Pb(Mg1/3Nb 2/3)O3 -PbTiO3 laminate composites", *J. Phys. D: Appl. Phys.*, **48**(46), 465002-465007, (2015). http://dx.doi.org/10.1088/0022-3727/48/46/465002

[16] Y. Wang, D. Gray, D. Berry, J. Gao, M. Li, J. Li, D. Viehland, "An Extremely Low Equivalent Magnetic Noise Magnetoelectric Sensor", *Adv. Mater.*, **23**(35), 4111–4114, (2011). http://dx.doi.org/10.1002/adma.201100773

[17] J. Gao, J. Das, Z. Xing, J. Li, D. Viehland, "Comparison of noise floor and sensitivity for different magnetoelectric laminates", *J. Appl. Phys.*, **108**(8), 084509-084511, (2010). http://dx.doi.org/10.1063/1.3486483

[18] V. Annapureddy, H. Palneedi, W.-H. Yoon, D.-S. Park, J.-J. Choi, B.-D. Hahn, C.-W. Ahn, J.-W. Kim, D.-Y. Jeong, J. Ryu, "A pT/√Hz sensitivity ac magnetic field sensor based on magnetoelectric composites using low-loss piezoelectric single crystals", *Sensor. Actuat. A: Phys*, **260** 206-211, (2017). http://dx.doi.org/10.1016/j.sna.2017.04.017

[19] Z. P. Xing, J. Y. Zhai, S. X. Dong, J. F. Li, D. Viehland, W. G. Odendaal, "Modeling and detection of quasi-static nanotesla magnetic field variations using magnetoelectric laminate sensors", *Meas. Sci. Technol.*, **19**(1), 015206-015214, (2008). http://dx.doi.org/10.1088/0957-0233/19/1/015206

[20] R. Jahns, H. Greve, E. Woltermann, E. Quandt, R. H. Knochel, "Noise Performance of Magnetometers With Resonant Thin-Film Magnetoelectric Sensors", *IEEE T. Instrum. Meas.*, **60**(8), 2995-3001, (2011). http://dx.doi.org/10.1109/TIM.2011.2122410

[21] X. Zhuang, C. Cordier, S. Saez, M. Lam Chok Sing, C. Dolabdjian, J. Gao, J.-F. Li, D. Viehland, "Theoretical analysis of the intrinsic magnetic noise spectral density of magnetostrictive-piezoelectric laminated composites", *J. Appl. Phys.*, **109**(12), 124512 - 124512-10, (2011). http://dx.doi.org/10.1063/1.3594714

[22] R. Jahns, H. Greve, E. Woltermann, E. Quandt, R. Knöchel, "Sensitivity enhancement of magnetoelectric sensors through frequency-conversion", *Sens. Actuators A-Phys.*, **183** 16-21, (2012). http://dx.doi.org/https://doi.org/10.1016/j.sna.2012.05.049

[23] J. Reermann, P. Durdaut, S. Salzer, T. Demming, A. Piorra, E. Quandt, N. Frey, M. Höft, G. Schmidt, "Evaluation of magnetoelectric sensor systems for cardiological applications", *Measurement*, **116** 230-238, (2018). http://dx.doi.org/10.1016/j.measurement.2017.09.047

[24] G. Sreenivasulu, U. Laletin, V. M. Petrov, V. V. Petrov, G. Srinivasan, "A permendur-piezoelectric multiferroic composite for low-noise ultrasensitive magnetic field sensors", *Appl. Phys. Lett.*, **100**(17), 173506-173510, (2012). http://dx.doi.org/10.1063/1.4705305

[25] G. Sreenivasulu, L. Y. Fetisov, Y. K. Fetisov, G. Srinivasan, "Piezoelectric single crystal langatate and ferromagnetic composites: Studies on low-frequency and resonance magnetoelectric effects", *Appl. Phys. Lett.*, **100**(5), 052901-052904, (2012). http://dx.doi.org/10.1063/1.3679661

[26] D. A. Burdin, D. V. Chashin, N. A. Ekonomov, L. Y. Fetisov, Y. K. Fetisov, G. Sreenivasulu, G. Srinivasan, "Nonlinear magneto-electric effects in ferromagnetic-piezoelectric composites", *J. Mag. Mag. Mat.*, **358–359** 98-104, (2014). http://dx.doi.org/10.1016/j.jmmm.2014.01.062

[27] D. A. Burdin, D. V. Chashin, N. A. Ekonomov, Y. K. Fetisov, A. A. Stashkevich, "High-sensitivity dc field magnetometer using nonlinear resonance magnetoelectric effect", *J. Mag. Mag. Mat.*, **405** 244-248, (2016). http://dx.doi.org/https://doi.org/10.1016/j.jmmm.2015.12.079

[28] Y. K. Fetisov, D. A. Burdin, D. V. Chashin, N. A. Ekonomov, "High-Sensitivity Wideband Magnetic Field Sensor Using Nonlinear Resonance Magnetoelectric Effect", *Sens. J., IEEE*, **14**(7), 2252-2256, (2014). http://dx.doi.org/10.1109/JSEN.2014.2309718

[29] L. Y. Fetisov, N. S. Perov, Y. K. Fetisov, G. Srinivasan, V. M. Petrov, "Resonance magnetoelectric interactions in an asymmetric ferromagnetic-ferroelectric layered structure", *J. Appl. Phys.*, **109**(5), 053908-053911, (2011). http://dx.doi.org/10.1063/1.3553640

[30] V. D. Kugel, G. Rosenman, D. Shur, "Piezoelectric properties of bidomain LiNbO3 crystals", *J. Appl. Phys.*, **78**(9), 5592-5596, (1995). http://dx.doi.org/10.1063/1.359681

[31] A. A. Timopheev, J. V. Vidal, A. L. Kholkin, N. A. Sobolev, "Direct and converse magnetoelectric effects in Metglas/LiNbO3/Metglas trilayers", *J. Appl. Phys.*, **114**(4), 044102-044108, (2013). http://dx.doi.org/10.1063/1.4816400

[32] J. V. Vidal, A. A. Timopheev, A. L. Kholkin, N. A. Sobolev, "Anisotropy of the magnetoelectric effect in tri-layered composites based on single-crystalline piezoelectrics", *Vacuum*, **122, Part B** 286-292, (2015). http://dx.doi.org/10.1016/j.vacuum.2015.06.022

[33] I. V. Kubasov, M. S. Timshina, D. A. Kiselev, M. D. Malinkovich, A. S. Bykov, Y. N. Parkhomenko, "Interdomain region in single-crystal lithium niobate bimorph actuators produced by light annealing", *Crystallogr. Rep.*, **60**(5), 700-705, (2015). http://dx.doi.org/10.1134/S1063774515040136

[34] I. V. Kubasov, A. M. Kislyuk, A. S. Bykov, M. D. Malinkovich, R. N. Zhukov, D. A. Kiselev, S. V. Ksenich, A. A. Temirov, N. G. Timushkin, Y. N. Parkhomenko, "Bidomain structures formed in lithium niobate and lithium tantalate single crystals by light annealing", *Crystallogr. Rep.*, **61**(2), 258-262, (2016). http://dx.doi.org/10.1134/S1063774516020115

[35] J. V. Vidal, A. V. Turutin, I. V. Kubasov, M. D. Malinkovich, Y. N. Parkhomenko, S. P. Kobeleva, A. L. Kholkin, N. A. Sobolev, "Equivalent Magnetic Noise in Magnetoelectric Laminates Comprising Bidomain LiNbO3 Crystals", *IEEE Trans. Ultrason. Ferroelectr. Freq. Control.*, **64**(7), 1102-1119, (2017). http://dx.doi.org/10.1109/TUFFC.2017.2694342

[36] J. N. Reddy, "Theory and Analysis of Elastic Plates and Shells", CRC Press, Taylor and Francis, 2006.

[37] S. Timoshenko, S. Woinowsky-Krieger, "Theory of plates and shells", McGraw-Hill, 1959.

[38] A. H. Meitzler, H. F. Tiersten, A. W. Warner, D. Berlincourt, G. A. Coquin, F. S. Welsh, "IEEE Standard on Piezoelectricity", *ANSI/IEEE Std 176-1987*, 1-74, (1988). http://dx.doi.org/10.1109/IEEESTD.1988.79638

[39] H. F. Tiersten, "Linear Piezoelectric Plate Vibrations", Springer US, 1969. http://dx.doi.org/10.1007/978-1-4899-6453-3

[40] V. Loyau, V. Morin, G. Chaplier, M. LoBue, F. Mazaleyrat, "Magnetoelectric effect in layered ferrite/PZT composites. Study of the demagnetizing effect on the magnetoelectric behavior", *J. Appl. Phys.*, **117**(18), 184102, (2015). http://dx.doi.org/10.1063/1.4919722

[41] V. Loyau, A. Aubert, M. LoBue, F. Mazaleyrat, "Analytical modeling of demagnetizing effect in magnetoelectric ferrite/PZT/ferrite trilayers taking into account a mechanical coupling", *J. Mag. Mag. Mat.*, **426** 530-539, (2017). http://dx.doi.org/https://doi.org/10.1016/j.jmmm.2016.11.125

[42] Z. Wu, Y. Wen, P. Li, in: 2012 IEEE International Ultrasonics Symposium, 2012, pp. 751-754. http://dx.doi.org/10.1109/ULTSYM.2012.0187

[43] D. T. H. Giang, P. A. Duc, N. T. Ngoc, N. T. Hien, N. H. Duc, "Enhancement of the Magnetic Flux in Metglas/PZT-Magnetoelectric Integrated 2D Geomagnetic Device", *J. Magn.*, **17**(4), 308-315, (2012). http://dx.doi.org/10.4283/JMAG.2012.17.4.308

[44] M. Guo, S. Dong, "A resonance-bending mode magnetoelectric-coupling equivalent circuit", *IEEE Trans. Ultrason. Ferroelectr. Freq. Control*, **56**(11), 2578-2586, (2009). http://dx.doi.org/10.1109/tuffc.2009.1346

[45] V. M. Petrov, G. Srinivasan, M. I. Bichurin, T. A. Galkina, "Theory of magnetoelectric effect for bending modes in magnetostrictive-piezoelectric bilayers", *J. Appl. Phys.*, **105**(6), 063911-063916, (2009). http://dx.doi.org/10.1063/1.3087766

[46] M. Bichurin, V. Petrov, "Modeling of Magnetoelectric Effects in Composites", Springer Netherlands, 2014. http://dx.doi.org/10.1007/978-94-017-9156-4

[47] V. M. Petrov, M. I. Bichurin, V. V. Zibtsev, S. K. Mandal, G. Srinivasan, "Flexural deformation and bending mode of magnetoelectric nanobilayer", *J. Appl. Phys.*, **106**(11), 113901-113906, (2009). http://dx.doi.org/10.1063/1.3264638

[48] K.-H. Cho, C.-S. Park, S. Priya, "Effect of intensive and extensive loss factors on the dynamic response of magnetoelectric laminates", *Appl. Phys. Lett.*, **97**(18), 182902-182904, (2010). http://dx.doi.org/10.1063/1.3511285

[49] Z. Xing, J. Li, D. Viehland, "Noise and scale effects on the signal-to-noise ratio in magnetoelectric laminate sensor/detection units", *Appl. Phys. Lett.*, **91**(18), 182902-182904, (2007). http://dx.doi.org/10.1063/1.2804118

[50] C. D. Motchenbacher, J. A. Connelly, "Low noise electronic system design", J. Wiley & Sons, 1993.

[51] R. S. Weis, T. K. Gaylord, "Lithium niobate: Summary of physical properties and crystal structure", *Appl. Phys. A: Mater. Sci. Process.*, **37**(4), 191-203, (1985). http://dx.doi.org/10.1007/bf00614817

[52] https://metglas.com/magnetic-materials/, last accessed in 15/03/2018.

[53] S. Dong, J. Zhai, J. Li, D. Viehland, "Near-ideal magnetoelectricity in high-permeability magnetostrictive/piezofiber laminates with a (2-1) connectivity.", *Appl. Phys. Lett.*, **89**(25), 252904-252906, (2006). http://dx.doi.org/10.1063/1.2420772

[54] Y. Wang, D. Hasanyan, M. Li, J. Gao, J. Li, D. Viehland, H. Luo, "Theoretical model for geometry-dependent magnetoelectric effect in magnetostrictive/piezoelectric composites", *J. Appl. Phys.*, **111**(12), 124513-124518, (2012). http://dx.doi.org/10.1063/1.4729832

[55] J. Zhai, S. Dong, Z. Xing, J. Li, D. Viehland, "Giant magnetoelectric effect in Metglas/polyvinylidene-fluoride laminates ", *Appl. Phys. Lett.*, **89**(8), 083507-083509, (2006). http://dx.doi.org/10.1063/1.2337996

[56] S. W. Meeks, J. C. Hill, "Piezomagnetic and elastic properties of metallic glass alloys Fe67CO18B14Si1 and Fe81B13.5Si3.5C2", *J. Appl. Phys.*, **54**(11), 6584-6593, (1983). http://dx.doi.org/10.1063/1.331893

[57] M. R. J. Gibbs, R. Watts, W. Karl, A. L. Powell, R. B. Yates, "Microstructures containing piezomagnetic elements", *Sensor. Actuat. A: Phys*, **59**(1), 229-235, (1997). http://dx.doi.org/https://doi.org/10.1016/S0924-4247(97)80180-X

[58] J. Gutierrez, A. Lasheras, J. M. Barandiaran, J. L. Vilas, M. S. Sebastian, L. M. Leon, "Improving the Magnetoelectric Response of Laminates Containing High Temperature Piezopolymers", *IEEE Trans. Magn.*, **49**(1), 42-45, (2013). http://dx.doi.org/10.1109/TMAG.2012.2220125

[59] G. Sreenivasulu, S. K. Mandal, S. Bandekar, V. M. Petrov, G. Srinivasan, "Low-frequency and resonance magnetoelectric effects in piezoelectric and functionally stepped ferromagnetic layered composites", *Phys. Rev. B*, **84**(14), 144426-144431, (2011). http://dx.doi.org/10.1103/PhysRevB.84.144426

[60] D. X. Chen, E. Pardo, A. Sanchez, "Demagnetizing factors for rectangular prisms", *IEEE Trans. Magn.*, **41**(6), 2077-2088, (2005). http://dx.doi.org/10.1109/TMAG.2005.847634

[61] C. Du-Xing, E. Pardo, A. Sanchez, "Demagnetizing factors of rectangular prisms and ellipsoids", *IEEE Trans. Magn.*, **38**(4), 1742-1752, (2002). http://dx.doi.org/10.1109/TMAG.2002.1017766

[62] Z.-Y. Zhang, Y.-y. Zhu, H.-f. Wang, L.-c. Wang, S.-n. Zhu, N.-b. Ming, "Domain inversion in LiNbO3 and LiTaO3 induced by proton exchange", *Physica B Condens. Matter*, **398**(1), 151-158, (2007). http://dx.doi.org/10.1016/j.physb.2007.05.011

[63] X. Cui, S. Dong, "Theoretical analyses on effective magnetoelectric coupling coefficients in piezoelectric/piezomagnetic laminates", *J. Appl. Phys.*, **109**(8), 083903, (2011). http://dx.doi.org/10.1063/1.3559301

[64] C.-M. Chang, G. P. Carman, "Modeling shear lag and demagnetization effects in magneto-electric laminate composites", *Phys. Rev. B*, **76**(13), 134116-134122, (2007). http://dx.doi.org/10.1103/PhysRevB.76.134116

[65] L. Guo, H. Zhang, R. Lu, G. Yu, "Magnetoelectric analysis of a bilayer piezoelectric/magnetostrictive composite system with interfacial effect", *Compos. Struct.*, **134** 285-293, (2015). http://dx.doi.org/https://doi.org/10.1016/j.compstruct.2015.08.064

[66] M. Silva, S. Reis, C. S. Lehmann, P. Martins, S. Lanceros-Mendez, A. Lasheras, J. Gutiérrez, J. M. Barandiarán, "Optimization of the Magnetoelectric Response of Poly(vinylidene fluoride)/Epoxy/Vitrovac Laminates", *ACS Appl. Mater. Interfaces*, **5**(21), 10912-10919, (2013). http://dx.doi.org/10.1021/am4031054

[67] H.-M. Zhou, Y.-H. Zhou, X.-J. Zheng, Q. Ye, J. Wei, "A general 3-D nonlinear magnetostrictive constitutive model for soft ferromagnetic materials", *J. Mag. Mag. Mat.*, **321**(4), 281–290, (2009). http://dx.doi.org/10.1016/j.jmmm.2008.09.012

[68] Y. Shen, K. L. McLaughlin, J. Gao, M. Li, J. Li, D. Viehland, "Effective optimization of magnetic noise for a Metglas/Pb(Zr,Ti)O3 magnetoelectric sensor array in an open environment", *Mater. Lett.*, **91**(0), 307-310, (2013). http://dx.doi.org/10.1016/j.matlet.2012.10.003

[69] S. Salzer, R. Jahns, A. Piorra, I. Teliban, J. Reermann, M. Höft, E. Quandt, R. Knöchel, "Tuning fork for noise suppression in magnetoelectric sensors", *Sensor. Actuat. A: Phys*, **237** 91-95, (2016). http://dx.doi.org/10.1016/j.sna.2015.10.040